Lab on a Chip

COMMUNICATION

View Article Online
View Journal | View Issue

Cite this: *Lab Chip*, 2025, **25**, 5129

Received 4th June 2025,
Accepted 16th July 2025

DOI: 10.1039/d5lc00553a

rsc.li/loc

Rocker or pump? Transcriptomic response of endothelial cells exposed to peristaltic pump-based unidirectional flow *vs.* rocker-induced bidirectional flow†

Negar Vahdani, [abc] Prateek Arora, [de] Lisette van Os, [a] Denise Ackermann,[a] Nadia Mercader [def] and Olivier T. Guenat [*acgh]

Rocking-platform perfusion systems rely on hydrostatic pressure differences to perfuse cells in organ-on-chip devices. These systems are popular due to their tubing-free design, which facilitates parallelization, an essential feature for drug discovery, precision medicine, and academic research. However, most of these systems generate bidirectional flow, which does not accurately replicate the physiological conditions experienced by endothelial cells (ECs) in the microvasculature. To address this limitation, pump-based systems are often employed to generate unidirectional flow, though they require external tubing, thereby limiting scalability compared to rocking platforms. In this study, under matched average flow rates, we compared the transcriptomic responses of endothelial cells exposed to flow generated either by a rocking platform or a peristaltic pump. Our results revealed distinct transcriptomic profiles induced by the two flow modalities, with hundreds of genes differentially expressed between the two conditions. After 4 hours of flow exposure, we observed an enrichment in signaling pathways including NF-κB, ERK, BMP and MAPK. Furthermore, after 24 hours of flow exposure, we identified significant changes in the genes involved in biological processes such as immune cell migration, angiogenesis and vascular and extracellular matrix remodeling, highlighting how different flow generated by a pump or a rocker can shape endothelial cell behavior at the molecular level.

Introduction

Organs-on-chips (OOCs) are revolutionizing *in vitro* modeling by precisely replicating the cellular microenvironment, including both biochemical and biophysical cues. A key feature of these platforms is the integration of flow, which is crucial in microfluidic systems for the perfusion of cultured cells.[1] However, a longstanding challenge in the field has been the reliance on external pumps connected to cumbersome tubing to deliver solutions into these systems. This technological hurdle hinders the scalability and widespread adoption of OOCs, particularly in high-throughput applications.

To address this issue, researchers have increasingly turned to rocking platforms, also called tilters, as a tubing-free alternative.[2] In these systems, fluid flows are based on gravitational forces resulting from periodic changes in platform orientation. Tilting the device creates a hydrostatic pressure gradient due to height differences between reservoirs, producing oscillatory (bidirectional) flow as the platform tilts alternately in both directions.[3] Users can modulate flow rates by controlling parameters such as tilt angle, frequency, and channel geometry, simplifying the experimental setups while enhancing scalability and operational efficiency. However, this convenience comes at a cost. The flow generated with the rocking platform is typically a non-constant bidirectional flow that diverges from the physiological unidirectional flow. In healthy conditions, flow through small-diameter vessels like capillaries is unidirectional and laminar, maintaining a low velocity shear stress essential for nutrient and oxygen exchange.[4] In contrast, bidirectional flow patterns are rarely observed *in vivo* in small vessels, and are often associated with pathological conditions, such as vascular obstruction and renal ischemia, where normal flow dynamics are disrupted.[5,6] Additionally, the flow rates achievable with rocking platforms

[a] *Organs-on-Chip Technologies Laboratory, ARTORG Center for Biomedical Engineering Research, University of Bern, Bern, Switzerland. E-mail: olivier.guenat@unibe.ch*
[b] *Graduate School for Cellular and Biomedical Sciences (GCB), University of Bern, Bern, Switzerland*
[c] *Multidisciplinary Center for Infectious Diseases (MCID), University of Bern, Bern, Switzerland*
[d] *Department of Developmental Biology and Regeneration, Institute of Anatomy, University of Bern, Switzerland*
[e] *Department of Biomedical Research, Cardiovascular Disease Program, University of Bern, Bern, Switzerland*
[f] *Centro Nacional de Investigaciones Cardiovasculares Carlos III, Madrid, Spain*
[g] *Department of Pulmonary Medicine, Inselspital, Bern University Hospital, University of Bern, Bern, Switzerland*
[h] *Department of General Thoracic Surgery, Inselspital, Bern University Hospital, University of Bern, Bern, Switzerland*
† Electronic supplementary information (ESI) available: Supplementary file, excel and video is available online. See DOI: https://doi.org/10.1039/d5lc00553a

are inherently limited by the small dimensions of microvascular channels and the modest tilt angles, which constrain the hydrostatic pressure gradient.

Wall shear stress is induced by a fluid flowing along a solid surface at the solid–liquid interface, which primarily affects endothelial cells (ECs) by triggering biomechanical signals *via* receptors on their membrane.[7] These mechanosensors predominantly consist of transmembrane proteins such as cell–cell junction proteins, adhesion molecules, receptors and ion channels, forming complexes that transmit stimuli to the nucleus, influencing hemostasis and EC phenotype.[8] Furthermore, fluid flow affects cell morphology, including cell polarization, organelle size, and gene expression, compared to a static condition.[9,10] Multiple mechanisms induced by shear stress impact vascular remodeling such as nitric oxide production, overexpression of junctional complexes like PECAM-1, and activation of the matrix metalloproteinases family.[11–13] Understanding how variations in flow conditions, such as bidirectional flow generated by rocking platforms compared to unidirectional flow generated by pump-based systems, impact cellular responses of ECs to wall shear stress is crucial for elucidating the physiological and pathological conditions. Winkelman *et al.*, showed enhanced vessel formation, connectivity, perfusability and barrier function under flow in a microvasculature model on chip.[14] Moreover, the flow profile further impacts EC phenotype and functions. For instance, Shuler *et al.* demonstrated that ECs exposed to bidirectional flow do not align with it, in contrast to those exposed to a unidirectional flow. This lack of alignment causes mechanoreceptors to become disoriented and unable to respond effectively.[15] Consistent with these findings, endothelial cells (ECs) exposed to unidirectional flow exhibited aligned orientation. They developed a robust barrier function, whereas those subjected to bidirectional flow displayed disorganized alignment, compromised junction integrity, and elevated levels of inflammatory markers such as IL-6 and IL-8.[16,17] ECs aligned to a 180° flow (reverse flow) respond to changes in flow direction at 45° and 90° through mechanisms involving NK-κB and endothelial nitric oxide synthesis.[18] Recently, Van Os *et al.* demonstrated that immune cells perfused in an endothelial lumen and exposed to a chemoattractant gradient extravasated across the endothelial barrier to the extracellular matrix (ECM) with a significant delay when exposed to a bidirectional flow compared to a unidirectional flow.[19] These findings underscore the importance of understanding how experimental conditions can influence endothelial cell (EC) responses. However, no study has yet demonstrated the impact of unidirectional and bidirectional flow on gene expression in endothelial cells cultured *in vitro*.

Our study addresses this question by comparing the transcriptomes of ECs exposed to peristaltic pump unidirectional flow with those exposed to rocker bidirectional flow. We assess the EC response after 4 and 24 hours. This comprehensive approach enhances our understanding of the molecular responses of endothelial cells exposed to two commonly used experimental fluidic setups.

Materials and methods

Microfluidic chip design and fabrication

The design and fabrication process of the microfluidic chip was reported in an earlier work by Van Os *et al.*[19] Briefly, the chip's design consists of three adjacent channels of different heights. The middle channel is 50 μm high, while the two adjacent channels are 200 μm high with a width of 500 μm. The middle channel was filled with 5 mg mL^{-1} fibrin hydrogel, which was maintained in place by phase guides, while the two adjacent channels were lined with endothelial cells. The microfluidic chip was produced by PDMS soft lithography. A mixture of a 10 : 1 ratio of PDMS (Dow Corning, USA) and curing agent was degassed and cured on the mold at 60 °C overnight. The cured PDMS was removed from the mold and the reservoirs were created using biopsy punches. The chips were then bonded to glass coverslips (VWR, USA) by activating the surfaces with a plasma O_2 (Henniker plasma, UK). Bonded chips were kept at 60 °C overnight to enhance the bonding strength. In the last step, the chips were sterilized for 15 min in an ozone/UV chamber (CoolClave, Genlantis, USA).

Cell culture

Human umbilical vein endothelial cells (HUVECs, Gibco, USA) were maintained in endothelial growth media (EGM-2, Lonza, Switzerland) with added supplements (EGM-2 BulletKit, Lonza, Switzerland) according to the manufacturer's instructions at 37 °C with 5% CO2. Cells were washed with DPBS (Sigma, USA) and treated with Accutase (Sigma, USA) for 5 min at 37 °C. Detached cells were centrifuged at 200 × g for 5 min. Experiments were performed with HUVECs at passages four to six.

Cell seeding on the microfluidic chip

The middle channel was filled with a final concentration of 5 mg mL^{-1} fibrin hydrogel before cell seeding. Fibrinogen (Sigma, USA) was mixed with 2 U thrombin solution in EBM2 (Sigma, USA) at a 1 : 1 ratio on ice. The central chamber of the chip was filled with hydrogel and incubated for 15 min at 37 °C to polymerize. After incubation, the adjacent channels were coated with polydopamine (PDA, Sigma, USA) for 24 h, followed by another coating solution containing 50 μg mL^{-1} bovine collagen (Advanced Biomatrix, USA) and 100 μg mL^{-1} bovine fibronectin (R&D Systems, USA) for two hours. After each step of the coating, channels were washed with sterile ddH_2O three times to remove the residues. HUVECs were suspended at a concentration of 4×10^7 cells per mL in EGM-2, and 1 μL of the solution was added in both adjacent channels and incubated for 15 min, allowing for cell attachment. Seeded chips were placed on a rocking platform (Mimetas, Netherlands) at a ±7° angle with a rocking interval of 8 min for 2.5 h. Floating non-adherent cells were flushed and replenished with supplemented EGM-2. Media was exchanged every day for 2 days until reaching the confluency of the endothelial cell layers.

Flow setups

Confluent endothelial cell layers were exposed to unidirectional or bidirectional flow for 4 or 24 hours.

Unidirectional flow setup. For the generation of unidirectional flow, a fluidic setup consisting of a peristaltic pump (Ismatec, Switzerland) connected each of the two adjacent channels, enabling a recirculating flow with a total volume of 200 μL. The flow rate was set to 2 μL min^{-1}, resulting in a shear stress of 0.1 dyn per cm^2 (0.01 Pa). A flow sensor (FS3, ELVEFLOW) was positioned downstream of the pump to measure the flow profile. The measurements were recorded with a sampling rate 10 Hz with a sensitivity of ±0.12 μL min^{-1}. The flow sensor and the peristaltic pump were individually calibrated prior to the experiments.

Bidirectional flow setup. The bidirectional flow was established using a rocker set at a 7° angle with 8 minutes intervals, resulting in a mean theoretical flow rate of 2.43 μL min^{-1} and an average shear stress of 0.1 dyn per cm^2 (0.012 Pa, see File S1† for the calculations of the flow rate and the average shear stress). Briefly, the time-dependent flow rate $Q(t)$ was calculated using a modified Poiseuille-based equation (eqn (1)), where ρ represents the fluid density, g the gravitational acceleration, w and h the width and height of the channel, L the length of the channel, L_R the distance between inlet and outlet reservoirs, μ the dynamic viscosity of the fluid, α the rocking angle, A the cross-sectional area of the reservoir, and t time. The height difference over time $\Delta h(t)$ was calculated using equation (eqn (2)). The driving pressure for the flow arises from the height difference between the fluid levels in the inlet and outlet reservoirs. This time-dependent height difference $\Delta h(t)$ was determined from the displaced volume, where $V(t)$ is the fluid volume displaced at time t. The initial height difference $\Delta h(0)$ is defined geometrically $\Delta h(0) = L_R \sin(\alpha)$, given by the tilting angle, a, and the distance between the inlet and outlet of the chip, L_R.

$$Q(t) = \frac{\rho g W H^3 L_R \sin(\alpha)}{12\mu L} e^{\frac{WH^3\rho g}{6\mu LA}t} \quad (1)$$

$$\Delta h(t) = \frac{2 \times V(t)}{A} \quad (2)$$

The flow rate was experimentally validated by monitoring perfused fluorescent latex beads (cat# L1030, Sigma Aldrich) with an average diameter of 2 μm, while the rocking platform was inclined at 7° for 8 minutes using 4× magnification using the M7000 EVOS microscope (Video S1†). The video was binarized, the background was removed, and the regions of interest were defined (the code is available on the GitHub repository **https://github.com/nvahdani/flow_ooc**). The beads were tracked, and the flow rate was calculated based on the obtained velocity.

The total volume of cell culture medium was set at 200μL and kept identical in both setups to ensure consistent dilution of cytokines and waste products, as well as an equal availability of nutrients and growth factors. Recirculating flow conditions were applied in both setups to maintain comparable environmental conditions.

Cytotoxicity assay

A cell viability assay was conducted to assess potential cell toxicity (LDH-Glo Cytotoxicity Assay, Promega). A bioluminescent method was used to measure released lactate dehydrogenase (LDH) in the supernatant. Briefly, the supernatant of each condition in three biological replicates was frozen in a storage buffer and mixed with the detection reagent according to the manufacturer's protocol. The luminescence was measured after incubation in technical duplicates (Tecan Reader Spark). The positive control was obtained by treating the samples with 10% Triton X-100 (Sigma-Aldrich, USA), inducing maximum cell death, and as the negative control, fresh cell culture medium was used. Data was normalized considering positive and negative control experiments. This involves subtracting the negative control from the average of the technical duplicates for each sample measurement and dividing by the positive control to calculate the percentage of cell death.

RNA isolation

Cell culture medium was removed, and the channels were washed with DPBS. Cells were detached and lysed enzymatically by adding 1-thioglycerol and lysis buffer solution. The RNA was isolated according to the manufacturer's protocol (ReliaPrepTM RNA Miniprep Systems, Promega) and pooled from two chips for the analysis.

Library preparation and RNA sequencing

The quantity and quality of purified total RNA were assessed using a Thermo Fisher Scientific Qubit 4.0 fluorometer with the Qubit RNA HS Assay Kit (Thermo Fisher Scientific, Q32855) and an advanced analytical fragment analyzer system using a Fragment Analyzer RNA Kit (Agilent, DNF-471), respectively.

Sequencing libraries were made with 50 ng input RNA using a Revelo mRNA-Seq for MagicPrep NGS kit A (Tecan, PN 30186623) according to the Revelo mRNA-Seq for MagicPrep NGS User Guide (Tecan publication number MO1535, v1). The resulting cDNA libraries were evaluated using a Thermo Fisher Scientific Qubit 4.0 fluorometer with the Qubit dsDNA HS Assay Kit (Thermo Fisher Scientific, Q32854) and an Agilent Fragment Analyzer (Agilent) with an HS NGS Fragment Kit (Agilent, DNF-474), respectively. Equimolar-pooled cDNA libraries were manually loaded onto one lane of an illumina NovaSeq 6000 SP Reagent Kit (100 cycles; illumina, 20028401) on an illumina NovaSeq 6000 instrument. The paired-end sequencing run produces on average, 29 million reads/library. The quality of the sequencing run was assessed using illumina sequencing analysis viewer (version 2.4.7) and all base call files were demultiplexed and converted into FASTQ files using illumina bcl2fastq conversion software v2.20.

Quality control and pre-processing

All downstream analysis on the sequenced data was performed using bash scripts and R version 4.3.2 in RStudio (2023.09.0 + 463 Posit Software, PBC). The sequencing quality was checked

using FastQC 0.11.0 for each sample before and after trimming and summarized with MultiQC.[20,21] The adapter sequence was removed using fastp 0.19.5.[22] Filtered data were aligned to the reference genome GRCh38 and the GTF file, version 111, from Ensembl using HISAT2, version 2.2.1.[23] FeatureCounts, subread package version 2.0.1., was used to assign the mapped reads to genomic features.[24]

Differential expression analysis

Deseq2, version 1.42.0, was used to identify differentially expressed genes in all conditions.[25] Low-expressed genes were filtered out by removing the gene counts below 5 across all the samples. To obtain the differentially expressed genes, the lfcShrink function with the ashr method, version 2.2.63, was employed.[26] Genes with log 2 fold expression changes greater than 0.585 and the adjusted *p*-value smaller than 0.05 were considered significant for the next steps. For the meta-analysis, bulk-RNA seq data from fresh EC cells isolated from human umbilical cords are obtained from Gene Expression Omnibus (GEO) under the GEO accession number GSE158081.[27] Combat-seq (sva 3.50.0) is used to correct the batch variations in the gene expression data. Downstream processing remains the same as described above.

Gene ontology enrichment analysis

Gene sets from each pairwise comparison with an adjusted *p*-value lower than 0.05 were enriched for the over- or under-represented gene ontology term using clusterProfiler 4.0.5 and represented in biomaRT annotation.[28,29] The gene ontology (GO) database was used with biological processes (BP), cellular component (CC), and molecular function (MF) annotations to perform the analysis and tidyverse R packages to handle and visualize the results.[30]

Immunocytochemistry and image analysis

All steps were carried out at room temperature unless otherwise mentioned. Chips were washed once with PBS and incubated for 15 min with 4% Paraformaldehyde (PFA, Invitrogen, USA). PFA was washed with PBS 3 times from the chip. Samples were permeabilized using 0.1% Triton X-100 for 10 min and washed 3 times with PBS. On the next step, cells were blocked with 2% BSA in PBS solution for 1 hour. After blocking, the primary antibody VE-Cadherin (R&D Systems, USA) was diluted in a 1 : 100 ratio in blocking solution and incubated at 4 °C overnight. Afterward, the primary antibody was washed 3 times with PBS. Cells were incubated for 2 h in a secondary antibody solution of donkey anti-Goat IgG conjugated with 546 Alexa Fluor (1 : 500, anti-goat 546, Invitrogen, USA), acti-stain phalloidin 670 (1 : 150, PHDN1, Denver, CO, USA) and Hoechst 33342 (1 : 1000, Sigma, USA), in 2% BSA blocking buffer. Finally, the chips were washed 3 times with PBS and Z-stack images were acquired on a confocal microscope (Zeiss LSM710, Zeiss, Germany). Brightfield images were taken by Nikon Eclipse Ts2 with 4× magnification and were analysed in Fiji v2.15.1 in technical duplicates and 3 biological replicates. Regions of interest (ROIs) were selected from the middle of the channels for further analysis. ROIs were pre-processed with a Gaussian blur to suppress high-frequency noise. Uneven illumination was corrected by contrast normalisation and histogram equalisation. Binary masks were generated with the global Yen thresholding algorithm, after which small artefacts were removed and internal holes filled using BioVoxxel. Continuous objects were separated with the Watershed transform and properties were extracted using analyze particles.

Statistics

Statistical analysis was performed using R version 4.3.2 in RStudio (2023.09.0 + 463 Posit Software, PBC). Shapiro–Wilk's test, two-sided pairwise *t*-test and one-way ANOVA were used to identify the data distribution and compare independent groups.

Results

Experimental design: endothelial cells exposed to different flow conditions

The microfluidic chip featured a central chamber filled with hydrogel, confined by two parallel phase guides, positioned between two adjacent channels (Fig. 1A), and was seeded with HUVECs. The use of adjacent channels under identical culture conditions enabled the maximization of the number of cells exposed to the same environment, facilitating the collection of sufficient cell quantities for the transcriptomics analysis. After generating a confluent cell layer in the microfluidic chip, the cells were exposed to either uni- or bidirectional flow for 4 or 24 hours. The unidirectional flow was established using a peristaltic pump in a recirculating fluidic circuit with a total volume of 200 μL and a flow rate of 2.03 μL min^{-1}, as measured by a flow sensor positioned downstream of the pump. The sensor's sensitivity enabled detection of the characteristic pulsatile pattern generated by the peristaltic pump (Fig. 1B). Bidirectional flow was generated by a rocking platform using the same volume to ensure a similar dilution effect of nutrients and paracrine signals. Experimental and theoretical flow rates are shown in Fig. 1C. Particle image velocimetry (PIV) was used to monitor the velocity of the fluorescent beads in the chip on a 7° inclined surface for an 8-minute interval. Both experimental and theoretical flow rates exhibited similar trends. A flow plateau around 1 μL min^{-1} may be attributed to increased capillary pressure and meniscus curvature at the reservoir walls. The surface tension became dominant, causing a flow rate plateau. The average wall shear stress in both flow conditions was maintained at 0.1 dyne per cm^2 (Fig. S1†).

The morphology and viability of endothelial cells under shear stress were assessed at 4- and 24-hour time points. Cell Morphological analysis on the brightfield images showed no overall effect on the cell count, total and average cell area, confluency percentage, perimeter-based shape factors

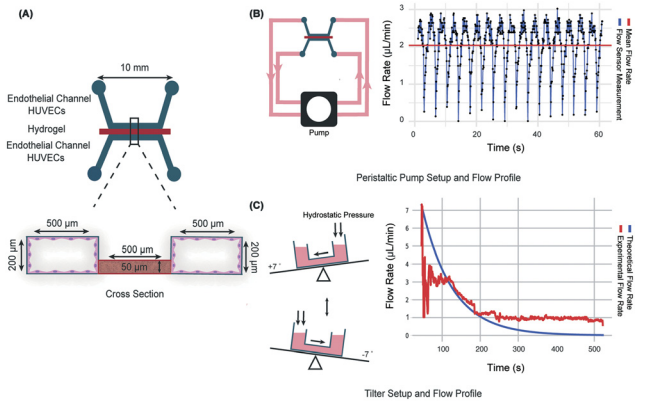

Fig. 1 Chip design and experimental setups. (A) Schematic of the PDMS microfluidic chip design and seeding layout. The middle channel is 50 μm high and filled with fibrin hydrogel, while endothelial cells are seeded on the adjacent channels with the dimensions of 200 μm width and 500 μm height and perfused with EGM-2 either on a rocker or with a peristaltic pump: peristaltic pump setup and the flow profile (B). Endothelial cells in the adjacent channels are connected to the recirculating tubing with a 200 μL cell culture medium per chip, generating unidirectional flow. Flow sensor measurements of the peristaltic pump over a 60-second interval show the pulsatile flow profile. Each black dot represents a measurement, and the red horizontal line indicates the mean flow rate detected by the sensor (2.03 μL min^{-1}). Rocker platform and the flow profile (C). Schematic of a gravity-driven flow with a tilting angle of ±7° demonstrating fluid flow driven by hydrostatic pressure in this system generating bidirectional flow. Measured flow rate (red) and theoretical flow rate (blue) over one interval (8 minutes) show similar flow rates, validating the calculated flow rate.

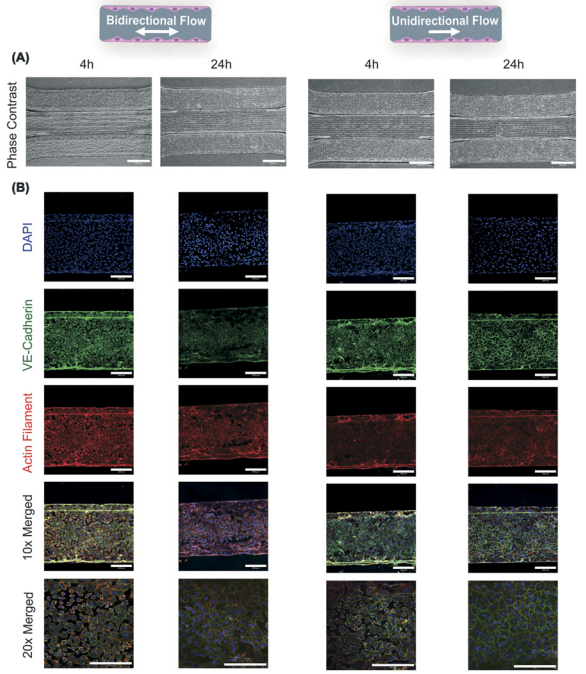

Fig. 2 Phase contrast and confocal microscopy of endothelial cell layers (A) phase contrast images of endothelial cell layers in the microfluidic device after 4 h and 24 h exposure to pump-based unidirectional flow or rocker-induced bidirectional flow (B) maximum intensity projection of the endothelial cells in all the conditions shows a fairly confluent layer of cells covering the lateral channels. The cells were stained for actin filament in red, VE-cadherin in green and Hoechst in blue in 10× and the merged channels in 10× and 20×. Scale bar: 200 μm.

(circularity, solidity), and orientation metrics (Fig. S1†). Elongation of ECs in the direction of the flow was shown to occur under high shear stress induced by laminar flow.[31] Cells were immunostained with VE-cadherin, phalloidin and Hoechst (Fig. 2). The maximum intensity projection of the stained samples revealed a fairly confluent lumen formation of endothelial cells, as corroborated by brightfield imaging. Additionally, the measurement of lactate dehydrogenase (LDH) levels in the supernatant showed no significant cell death attributable to either flow conditions at both time points (Fig. S2†). These results indicate that the flow exposure does not induce cytotoxic effects and is suitable for further experiments.

Comparative gene expression of endothelial cells exposed to peristaltic pump-based unidirectional flow *vs.* rocker-induced bidirectional flow

Having established the cell culture, the next step was investigating transcriptomic changes induced by either rocker bidirectional flow or pump-driven unidirectional flow by performing bulk RNA sequencing (RNA seq) on endothelial cells isolated from the microfluidic devices. Principal component analysis (PCA) revealed distinct expression profiles between cells exposed to pump-driven unidirectional and rocker induced-bidirectional flow at 24 hours (Fig. 3A). The separation of data was less pronounced at the 4 hour time point. A clustered heatmap of differentially expressed genes, normalized by z-score across all samples, highlights these differences, particularly at 24 hours (Fig. 3B). Notably, endothelial cells exposed to bidirectional flow exhibited a relatively homogeneous gene expression pattern across both time points and replicates. To further characterize these differences, we conducted differential expression analysis for each flow condition at both 4 and 24 hours. The number of differentially expressed genes (DEGs) from pairwise comparison conditions was visualized using box plots (Fig. 3C). Consistent with the trend observed in the PCA results, 365 DEGs were identified after 4 hours of flow exposure, including 265 upregulated and 100 downregulated genes (Table S1†). At 24 hours, this number increased to 761 DEGs, with 310 upregulated and 451 downregulated genes (Table S1†). These findings suggest that flow, generated by the rocker or the pump, significantly influences gene expression of HUVECs, with more pronounced transcriptional changes emerging over longer exposure durations.

Differential gene expression and enriched biological processes induced by the flow types

Upregulated and downregulated genes were visualized using volcano plots, comparing the gene expression profile of HUVECs exposed to uni and bidirectional flow generated by the pump and rocker, respectively 4 hours (Fig. 5A) and 24 hours (Fig. 4A). Gene ontology (GO) annotation was employed to identify overrepresented biological processes among the differentially expressed genes (Table S2†). At the 24-hour, the

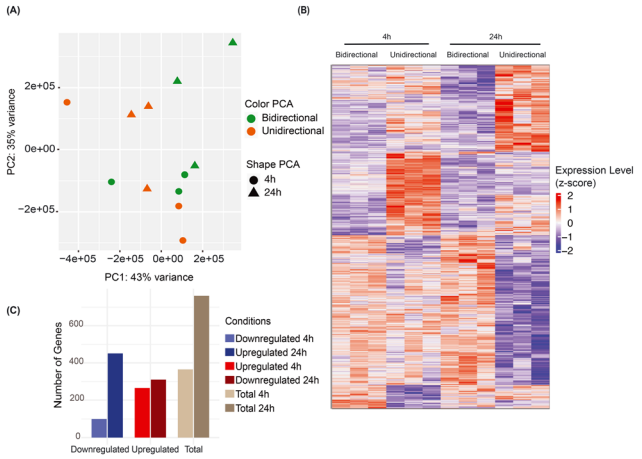

Fig. 3 Gene expression profile of HUVECs exposed to uni- and bidirectional flow driven by a peristaltic pump and rocker, respectively. (A) PCA plot showing the distribution of samples exposed to either uni- or bidirectional flow. The plot indicates a distinct gene expression profile of HUVECs at 24 h. (B) The heatmap represents gene expression values normalized by z-score in a color gradient from lowly expressed genes in blue and highly expressed genes in red. A distinct expression pattern is visible when comparing pump-based unidirectional flow and rocker-induced bidirectional flow. (C) The total number of altered genes, upregulated and downregulated genes for each time point are graphed.

top 15 enriched biological processes were mainly involved in DNA replication, including chromosome segregation, cell cycle-dependent and DNA replication processes (Fig. S3A†). Additional enriched pathways at 24 hours included those associated with angiogenic sprouting, vascular development, cell migration, tissue regeneration, regulation of cytokines and chemokines, microtubule processes and cyclin-dependent protein serine/threonine kinase activity (Fig. 4B). A heatmap displaying differentially expressed genes between pump-based unidirectional and rocker-induced bidirectional flow conditions at 24 hours, normalized by z-score, is shown in Fig. 4C. The heatmap includes annotations for selected genes and their associated enriched pathways. Several genes involved in cell migration were differentially expressed, such as ITGA2, KITLG and ADAM17, which were upregulated in unidirectional flow, and VCAM1 was elevated in bidirectional flow. Moreover, angiogenic growth factors, such as FGF16, PFG and its receptor FLT1 (VEGFR1), showed higher expression levels in response to unidirectional flow. At the 4-hour time point, enriched pathways included those associated with ERK, JNK, BMP and MAPK signaling pathways, as well as SMAD proteins (Fig. 5B) (Table S2†). RK, SMAD and KLF2/KLF4 are intracellular transduction proteins that adapt cell homeostasis to mechanical forces.[32] TGF-β2, one of the intracellular transduction pathways, was upregulated in ECs on rocker after 24 h. He intensity of TGF-β2 response is dependent on the cue properties and results in downstream SMAD protein activation.[33] Differentially expressed genes, normalized by z-score, are shown in a heatmap (Fig. 5C), with annotations highlighting genes involved in these enriched biological processes. HUVECs exposed to 4 hours of unidirectional flow showed higher expression of key transcription factors, such as MEF2A and KLF4. In contrast, several genes, including BMP4 (bone morphogenetic protein 4), BMPER (BMP endothelial cell precursor–derived regulator) were downregulated under unidirectional flow conditions, generated by the pump setup.[34,35] In addition, BMP receptor 2 which has been shown to play a role in the phenotype differentiation of ECs to tip cells was overexpressed at 4 hours timepoint in this setup.[36] Interestingly, altered expression of certain genes, such as PTGS2, ANGPT2, IL11 and BMP4, was observed at both 4 and 24 hours, suggesting early and sustained activation. Upregulation of BMP4, IL11 and PTGS2 suggests that the SMAD-FOXO1 pathway is already being switched on in low shear stress unidirectional flow, as previously reported by Mendez *et al.* studying oscillatory shear in human aortic endothelial cells.[37] The top 15 enriched pathways at 4 hours were primarily related to tissue development and morphogenesis processes (Fig. S3B†). In summary, our gene expression data suggest a temporal shift in pathways enrichment, with early activation of cell signaling-related pathways at 4 hours, shifting towards cytoskeleton remodeling and angiogenesis-related processes at 24 hours.

Transcriptomic comparison of *in vivo* cells with cells exposed to different flow types

Under healthy *in vivo* conditions, endothelial cells in the microvasculature experience unidirectional laminar shear forces. Therefore, a meta-analysis was performed to compare the gene expression profiles of freshly isolated HUVECs from Afshar *et al.*[27] with *in vitro* cultures exposed to uni- and bidirectional flow. The effect of varying experimental designs, such as RNA extraction and sequencing protocols, was normalized using the ComBat_seq batch correction method. Principal component analysis revealed a distinct population for the *in vivo* data, while the *in vitro* data clustered more closely (Fig. 6A). The number of differentially expressed genes was similar when comparing flow-exposed cells to *in vivo* HUVECs (Fig. 6B). Importantly, when comparing the gene expression profile of the *in vivo* umbilical cells to *in vitro* cells exposed to pump-driven unidirectional flow and rocker-induced bidirectional flow, the number of genes common to both conditions exceeded those unique to each specific condition (Fig. 6C). This, along with the PCA, suggests that the *in vivo* samples show a distinct gene expression profile compared to the *in vitro* samples.

Discussion

Most organ-on-a-chip (OOC) systems rely on continuous perfusion to replicate physiological microenvironments, typically using rocking platforms or pump-based systems, each with specific strengths and trade-offs. In vascular models, endothelial cells are cultured under flow to mimic *in vivo* conditions, as shear stress significantly alters endothelial gene expression in a magnitude- and time-dependent manner.[38–41] In recent years, rocking platforms, relying on hydrostatic pressure differences to drive perfusion, have gained popularity as a low-

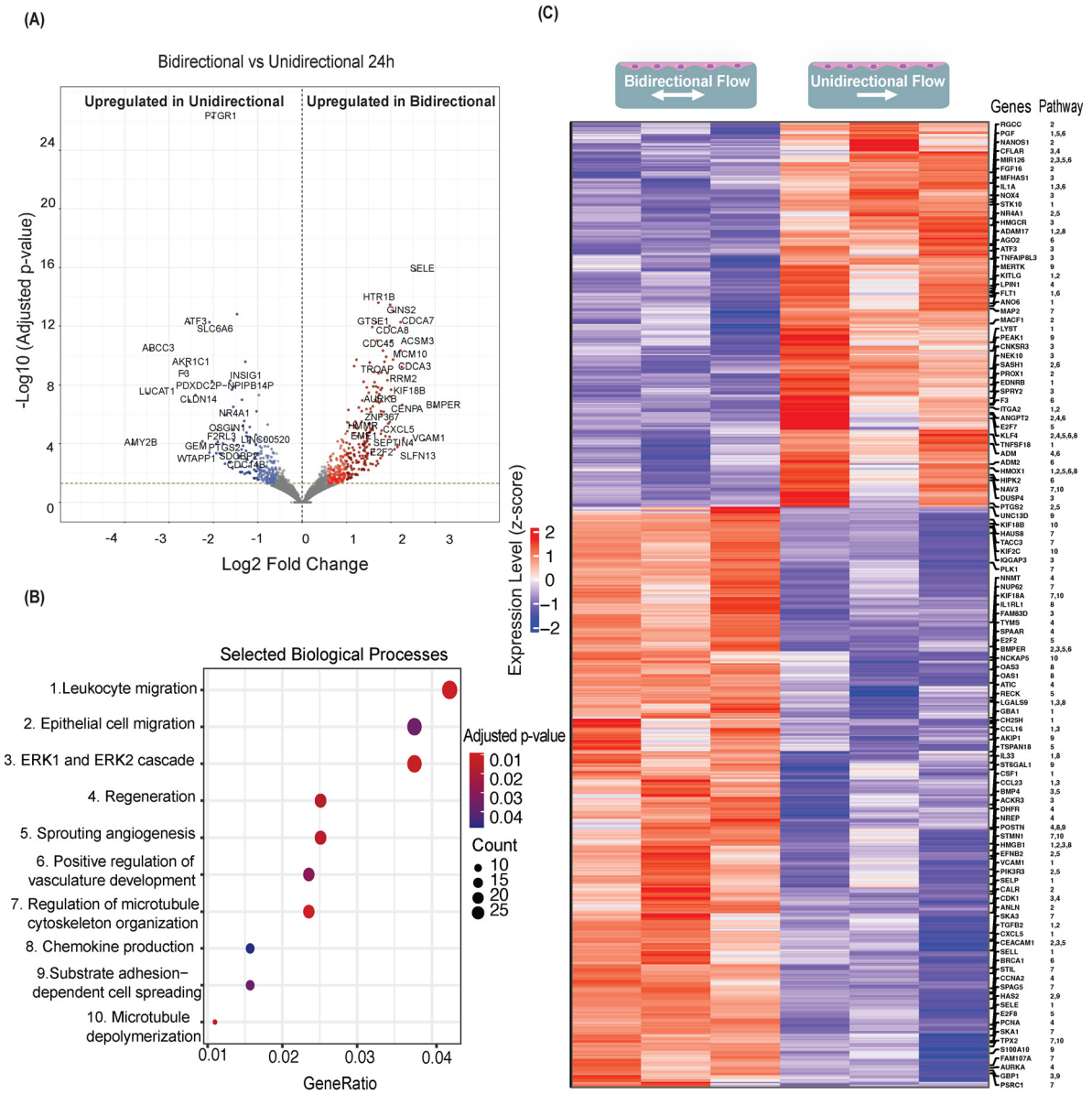

Fig. 4 Differential gene expression and enriched biological processes comparing uni *vs.* bidirectional flow driven by peristaltic pump or rocker after 24 h of flow exposure. (A) The volcano plot illustrates upregulated genes exposed to unidirectional flow in dark red (log fold change of 2) and light red (log fold change of 1.5). Downregulated genes are shown in dark blue (log fold change of 2) and light blue (log fold change of 1.5). A total of 761 genes, 310 upregulated and 451 downregulated, were altered. (B) Gene ontology (GO) analysis shows selected biological processes altered in HUVECs exposed to flow after 24 h. The GO plot represents the number of genes assigned to each enriched pathway and the adjusted *p*-value. (C) Heatmap showing the expression pattern across samples of the differentially expressed genes in 24 h timepoint. The number annotated with the genes corresponds to the pathways where the genes can be observed in GO of biological process.

maintenance alternative to traditional pump-based systems.[3] These perfusion systems are favored for their simplicity, the elimination of cumbersome tubing, and compatibility with high-throughput applications.[13] However, the bidirectional and non-physiological nature of the flow they generate may result in altered or inconsistent cellular responses. Building on our previous work, we investigated how gene expression of HUVECs is affected by rocker-induced bidirectional flow and peristaltic pump-based unidirectional flow. Although cells were exposed to the same average shear stress of 0.1 dyn per cm^2 for either 4 hours or 24 hours, the rocker induces a wider range of shear stress, ranging from 0.29 dyn per cm^2 to 0.041 dyn per cm^2; therefore, cells may respond differently to these distinct mechanical stimulation patterns. While the peristaltic pump system introduced oscillatory components with 0.3 Hz frequency compared to an 8-minute interval of the rocker, that represents an additional variable, studies suggest cellular responses to such low-frequency oscillations at our shear stress levels are likely minimal.[42–44] Other variables, such as the cell culture medium volume of 200 μL were maintained constant across all conditions, ensuring that dilution factors (including cytokines and metabolic waste) were equivalent between both

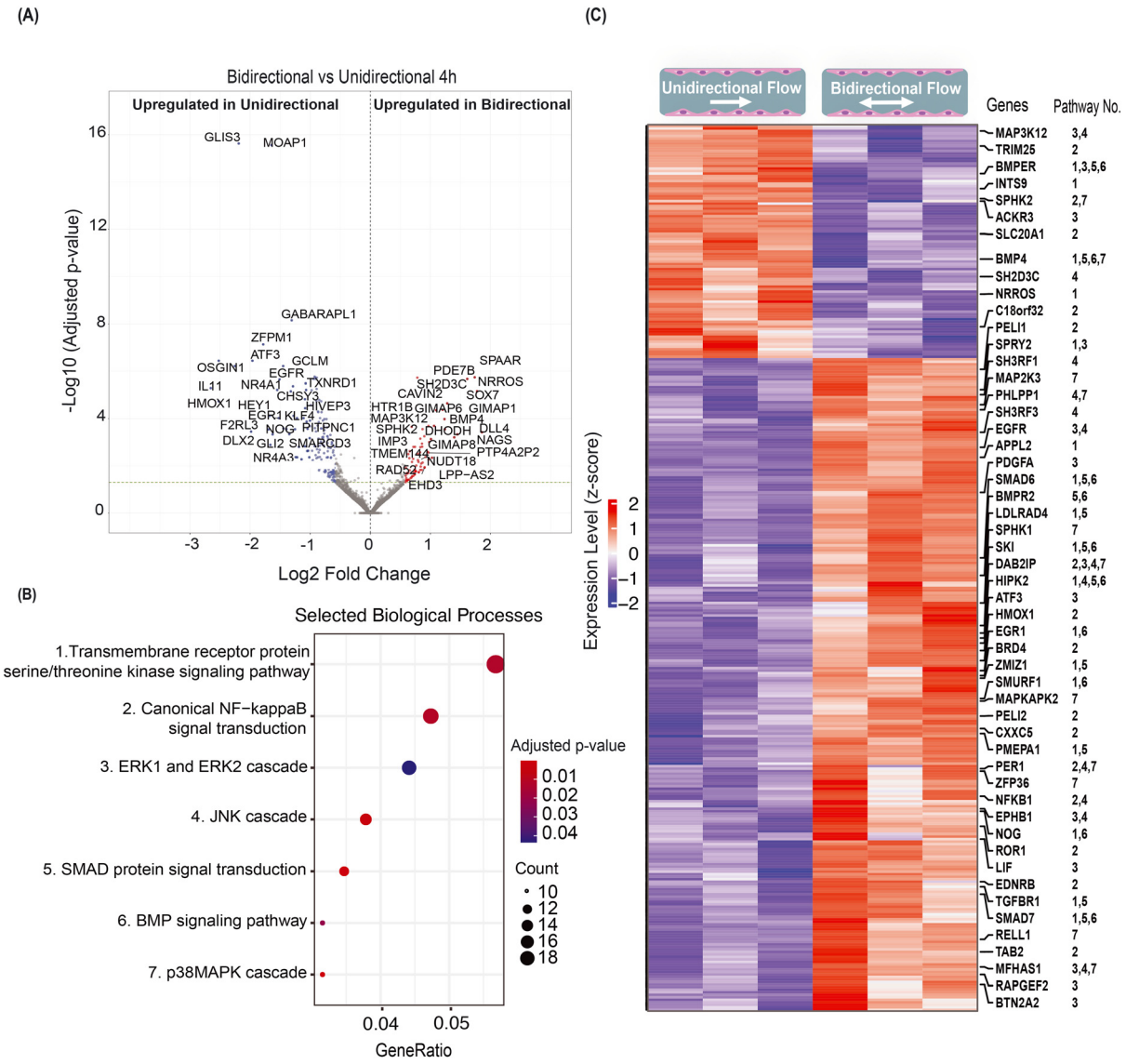

Fig. 5 Differential gene expression and enriched biological processes comparing uni- *vs.* bidirectional flow driven by peristaltic pump or rocker after 4 h of exposure. (A) The volcano plot illustrates upregulated genes with a log fold change of 2 (dark red) and a log fold change of 1.5 (light red). Downregulated genes are shown in dark blue (log fold change of 2) and in light blue (log fold change of 1.5). A total of 365 genes, 265 upregulated and 100 downregulated, were altered. (B) Gene ontology (GO) analysis shows selected biological pathways in HUVECs exposed to flow after 4 h. The GO plot represents the number of genes assigned to each enriched pathway and the adjusted *p*-value. (C) Heatmap showing the expression pattern across samples of the differentially expressed genes in 4 h timepoint. The number associated with the genes corresponds to the pathways where those genes can be observed the GO of biological process.

setups. We observed substantial differences in gene expression between the two flow types, with a hundred genes differentially expressed. These gene expression changes affected various biological pathways, including immune cell transmigration, ECM remodeling, angiogenesis, and DNA replication.

Rocker or pump-induced flow direction and immune cell transmigration

As previously demonstrated by our group, bidirectional flow significantly delays the transmigration of peripheral blood mononuclear cells (PBMCs) across an endothelial barrier.[19] Leukocyte recruitment involves a multi-step process: initial low-affinity rolling on the endothelial cell layer, high-affinity adhesion, and subsequent transmigration through the endothelial layer.[45] Various adhesion molecules and cytokines participate in these processes. During the rolling phase, leukocytes interact with endothelial cells expressing vascular cell adhesion molecule-1 (V-CAM-1) and members of the selectin family: P-selectin (SELP), E-selectin (SELE) and L-selectin (SELL).[46] Our findings indicate that these adhesion molecules are upregulated in endothelial cells exposed to rocker flow, which may enhance low-affinity interactions between immune cells and the endothelial cells. Notably, reduced

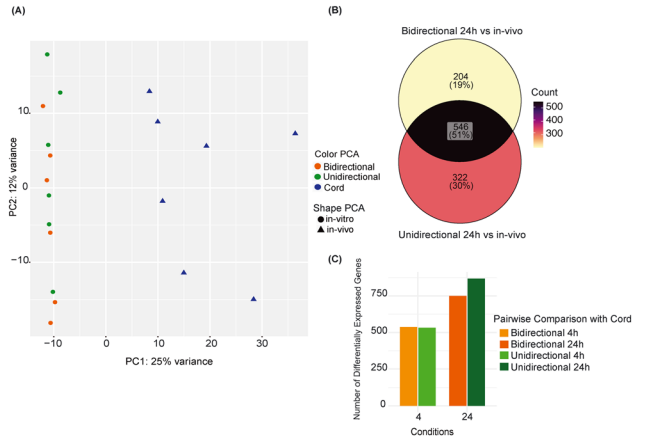

Fig. 6 Transcriptomic meta-analysis of *in vivo* and *in vitro* data exposed to uni- and bidirectional flow induced by peristaltic pump or rocker. (A) The PCA plot represents the *in vivo* and *in vitro* data clustering with no tendency toward a specific flow type. (B) A Venn diagram suggests that the same gene set was altered in all the conditions. (C) The barplot shows the number of differentially expressed genes when comparing flow types with freshly isolated cord blood-derived HUVECs. All conditions exhibit nearly an equal number of differentially expressed genes.

BMPER levels have been shown to drive a similar pro-adhesive phenotype, upregulating VCAM-1, ICAM-1 and selectins, and boosting leukocyte adhesion both *in vitro* and *in vivo*.[47] Integrins, another family of adhesion molecules, are critical for transitioning from the rolling to the arresting process with high-affinity binding. Their activation, triggered by external and internal mechanical cues, regulates leukocyte arrest and transendothelial migration. Various integrins facilitate immune cells' adhesion and amoeboid migration, while also regulating cell proliferation and homeostasis.[48] We observed upregulation of ITGA2, ITGA10, ITGA11, and the KIT ligand (KITLG) under unidirectional flow, suggesting transcriptional modulation of adhesion-related pathways in this flow regime. Notably, the interaction between KITLG and mechanosensitive integrins was shown to promote mast cell adhesion.[49]

In summary, our results indicate that different flow profiles, rocker-induced bidirectional flow and unidirectional flow of the peristaltic pump activate gene expression related to distinct pathways in the immune cell migration processes. Thereby, potentially altering immune cell dynamics within microphysiological systems.

Endothelial angiogenesis and ECM remodeling under flow dynamics

Endothelial angiogenesis is closely regulated by ECM remodeling, a process significantly influenced by mechanical forces such as shear stress.[50] In our study, pump-driven unidirectional flow led to the upregulation of matrix metalloproteinases (MMPs), mainly MMP-1 and MMP-10, as well as a member of the ADAMTS (a disintegrin and metalloproteinase with thrombospondin motifs) family. These enzymes are critical regulators of ECM homeostasis, responsible for degrading structural components such as collagen, fibronectin, and laminin.[51] ECM remodeling directly impacts key angiogenesis aspects, such as angiogenic sprouting, neovascularization, tube formation and cell migration[52] as well as the interplay between endothelial cells, pericytes, and vascular smooth muscle cells.[33] The observed upregulation of these matrix-modifying genes under pump-driven unidirectional flow suggests enhanced ECM remodeling, which may contribute to a more permissive microenvironment that supports EC proliferation, migration and angiogenesis.[53] Furthermore, higher gene expression of CEACAM1 and MACF1 under rocker-induced bidirectional flow, which are involved in microvasculature tube formation and endothelial cell migration, indicates that distinct flow patterns differentially influence genes involved in angiogenic pathways and structural reorganization within the vascular niche.

Beyond ECM remodeling, shear stress also influences the transcriptional state and cell fate.[41,54] Under unidirectional flow, the transcription factor MEF2A was upregulated, which plays a key role in initiating Notch signaling and activating KLF4 (Krüppel-like factor) in a flow-dependent manner.[55] The early upregulation of MEF2A, together with the Notch pathway components, HEY1 and DLL1, suggests that pump-driven unidirectional flow promotes vasculogenesis and angiogenesis. HEY1, a downstream target of Notch signaling, and DLL1, were both upregulated after 4 hours of flow exposure, highlighting their involvement in early vascular development.[56–58] Additionally, several members of the KLF family, such as KLF4, KLF11 and KLF13, were upregulated under pump setup experiments, which is consistent with previous findings, which showed that KLF4 expression was induced by pulsatile laminar shear stress.[59] The sustained upregulation of KLF4 at both 4 and 24 hours, along with the upregulation of VEGFR1, its ligands, and placenta growth factor (PFG), indicates a prolonged transcriptional response to pump-driven unidirectional flow.[60,61]

Enhanced BMP signaling pathway under rocker-induced bidirectional flow

Under rocker-induced bidirectional flow, several enriched signaling pathways were upregulated compared to pump-driven unidirectional flow. Among them are BMP4, members of the transforming growth factor-β (TGF-β2) and BMPER. BMP4 participates in adult vessel formation, and BMPER is a dose-dependent activator that regulates the angiogenic process.[34,62] The concurrent downregulation of BMP pathway inhibitors, SMAD6 and SMAD7, aligns with the upregulation of BMP and BMPER under the rocker flow setup.[63] BMP signaling can proceed *via* canonical (SMAD-dependent), and non-canonical (SMAD-independent) pathways including ERK, JNK, and p38 MAPK. Notably, significant JNK and p38 MAPK activity changes were observed in response to rocker-induced bidirectional flow.[35,64]

Meta-analysis: physiological relevance of rocker or pump-induced flow direction

The meta-analysis comparing transcriptomic data with previously published *in vivo* data revealed limited overlap between the two studies. This was expected as the comparison involved HUVECs from one donor cultured in a simplified fluidic model with very low shear stress, unlike human umbilical endothelial cells embedded in their native tissue. As a result, the meta-analysis demonstrated only a modest overlap, highlighting the differences in experimental setups and donor variability. Future studies should incorporate the specific conditions central to this environment to more accurately replicate an umbilical cord, such as the interaction between multiple cell types and ECM components.

Conclusions

This study explored the differences between pump-driven unidirectional and rocker-induced bidirectional flow in commonly implemented flow setups within OOC systems. While a fully controlled comparison between the two experimental conditions was not entirely feasible due to variations in flow parameters and the non-constant flow in the rocker compared to the pulsatile flow generated by the peristaltic pump, we aimed to highlight how the choice of flow configuration in OOC systems can significantly influence biological outcomes, depending on the specific research question. Rocking platforms, which have gained popularity for their simplicity and suitability for parallel experimentation, should be approached cautiously. Recent developments in microfluidic chip design that enable unidirectional flow using rockers represent a promising advancement in addressing this limitation.[65,66] An additional limitation in incorporating the rocking platforms lies in their restricted capacity to generate physiologically relevant shear stress. This constraint is due to intrinsic geometric limitations and the viscosity of the cell culture medium, where increasing the tilting angle fails to produce flow rates sufficient to match those found *in vivo*, particularly within smaller vessels. In fact, in these systems, pressure is governed by hydrostatic pressure, meaning that a 100-fold increase in shear stress required to obtain physiological shear stress necessitates a 100-fold increase in hydrostatic pressure difference, which is not feasible. Future work could shorten the rocking cycle, avoiding the flow rate drop in each interval. Furthermore, it is noteworthy that long-term shear-stress exposure of endothelial cells may result in a different gene-expression profile. Finally, the striking transcriptomic differences and the wide range of enriched pathways influenced by flow type highlight the significance of this issue. Our findings suggest that previous results obtained under non-constant rocker-induced bidirectional flow conditions may need to be re-evaluated or validated using pump-driven unidirectional flow.

Data availability

The raw data for bulk RNAseq produced in this analysis can be accessed through the NCBI Gene Expression Omnibus (GEO) with accession number GSE272273. The code used for the analysis is available on the GitHub repository **https://github.com/nvahdani/flow_ooc**.

Author contributions

NV, LvO and OG conceived and developed the study. NM provided conceptual input on transcriptomic design. NV performed the cell culture experiments and collected the data. NV, PA and OG analyzed the data. NV and PA carried out the NGS sequencing and interpreted the data. NV wrote the manuscript. DA analyzed the particle tracking video. PA, NM and OG thoroughly revised the manuscript. All authors read the manuscript and approved the final version.

Conflicts of interest

The authors declare that the research was conducted in the absence of any commercial or financial relationships that could be construed as a potential conflict of interest.

Acknowledgements

The writing of the manuscript was supported by a Large Language Model (ChatGPT v3.5, OpenAI Inc, California, USA) to improve the text's grammar and optimize the choice of words. Microscopy was performed on equipment supported by the Microscopy Imaging Center (MIC), University of Bern, Switzerland. The Next Generation Sequencing Platform, University of Bern conducts the quality control assessments, generation of libraries and sequencing. OG recieved funding from the Multidisciplinary Center for Infectious Diseases (MCID) of the University of Bern (MA-09). NM received funding from the European Union's Horizon 2020 research and innovation programme under grant agreement No 874764 – H2020-SC12019-Single-Stage-RTD REANIMA-874764.

Notes and references

1 C. M. Leung, P. De Haan, K. Ronaldson-Bouchard, G. A. Kim, J. Ko and H. S. Rho, *et al.*, A guide to the organ-on-a-chip, *Nat. Rev. Methods Primers*, 2022, **2**(1), 33.
2 B. Zhang, A. Korolj, B. F. L. Lai and M. Radisic, Advances in organ-on-a-chip engineering, *Nat. Rev. Mater.*, 2018, **3**(8), 257–278.
3 J. H. Sung, C. Kam and M. L. Shuler, A microfluidic device for a pharmacokinetic–pharmacodynamic (PK–PD) model on a chip, *Lab Chip*, 2010, **10**(4), 446.
4 E. M. Wasson, K. Dubbin and M. L. Moya, Go with the flow: modeling unique biological flows in engineered in vitro platforms, *Lab Chip*, 2021, **21**(11), 2095–2120.
5 M. K. Vormann, L. M. Tool, M. Ohbuchi, L. Gijzen, R. Van Vught and T. Hankemeier, *et al.*, Modelling and Prevention

of Acute Kidney Injury through Ischemia and Reperfusion in a Combined Human Renal Proximal Tubule/Blood Vessel-on-a-Chip, *Kidney360*, 2022, **3**(2), 217–231.

6 J. M. Wilkinson, A review of complex in vitro cell culture stressing the importance of fluid flow and illustrated by organ on a chip liver models, *Front. Toxicol.*, 2023(5), 1170193.

7 D. A. Chistiakov, A. N. Orekhov and Y. V. Bobryshev, Effects of shear stress on endothelial cells: go with the flow, *Acta Physiol.*, 2017, **219**(2), 382–408.

8 R. Santamaría, M. González-Álvarez, R. Delgado, S. Esteban and A. G. Arroyo, Remodeling of the Microvasculature: May the Blood Flow Be With You, *Front. Physiol.*, 2020, **11**, 586852.

9 U. M. Sonmez, Y. W. Cheng, S. C. Watkins, B. L. Roman and L. A. Davidson, Endothelial cell polarization and orientation to flow in a novel microfluidic multimodal shear stress generator, *Lab Chip*, 2020, **20**(23), 4373–4390.

10 K. Kulthong, G. J. E. J. Hooiveld, L. Duivenvoorde, I. Miro Estruch, V. Marin and M. Van Der Zande, *et al.*, Transcriptome comparisons of in vitro intestinal epithelia grown under static and microfluidic gut-on-chip conditions with in vivo human epithelia, *Sci. Rep.*, 2021, **11**(1), 3234.

11 J. A. Espina, M. H. Cordeiro, M. Milivojevic, I. Pajić-Lijaković and E. H. Barriga, Response of cells and tissues to shear stress, *J. Cell Sci.*, 2023, **136**(18), jcs260985.

12 L. Zheng, Y. Huang, W. Song, X. Gong, M. Liu and X. Jia, *et al.*, Fluid shear stress regulates metalloproteinase-1 and 2 in human periodontal ligament cells: Involvement of extracellular signal-regulated kinase (ERK) and P38 signaling pathways, *J. Biomech.*, 2012, **45**(14), 2368–2375.

13 Y. Juste-Lanas, S. Hervas-Raluy, J. M. García-Aznar and A. González-Loyola, Fluid flow to mimic organ function in 3D in vitro models, *APL Bioeng.*, 2023, **7**(3), 031501.

14 M. A. Winkelman, D. Y. Kim, S. Kakarla, A. Grath, N. Silvia and G. Dai, Interstitial flow enhances the formation, connectivity, and function of 3D brain microvascular networks generated within a microfluidic device, *Lab Chip*, 2022, **22**(1), 170–192.

15 Y. I. Wang and M. L. Shuler, UniChip enables long-term recirculating unidirectional perfusion with gravity-driven flow for microphysiological systems, *Lab Chip*, 2018, **18**(17), 2563–2574.

16 Y. Yang, P. Fathi, G. Holland, D. Pan, N. S. Wang and M. B. Esch, Pumpless microfluidic devices for generating healthy and diseased endothelia, *Lab Chip*, 2019, **19**(19), 3212–3219.

17 M. Ansarizadeh, H. T. Nguyen, B. Lazovic, J. Kettunen, L. De Silva and R. Sivakumar, *et al.*, Microfluidic vessel-on-chip platform for investigation of cellular defects in venous malformations and responses to various shear stress and flow conditions, *Lab Chip*, 2025, **25**(4), 613–630.

18 C. Wang, B. M. Baker, C. S. Chen and M. A. Schwartz, Endothelial Cell Sensing of Flow Direction, *ATVB*, 2013, **33**(9), 2130–2136.

19 L. Van Os, J. Yeoh, G. Witz, D. Ferrari, P. Krebs and Y. Chandorkar, *et al.*, Immune cell extravasation in an organ-on-chip to model lung inflammation, *Eur. J. Pharm. Sci.*, 2023, **187**, 106485.

20 Andrews S., FastQC: a quality control tool for high throughput sequence data [Internet]. 2010 [cited 2024 May 21]. Available from: **https://www.bioinformatics.babraham.ac.uk/projects/fastqc/**.

21 P. Ewels, M. Magnusson, S. Lundin and M. Käller, MultiQC: summarize analysis results for multiple tools and samples in a single report, *Bioinformatics*, 2016, **32**(19), 3047–3048.

22 S. Chen, Y. Zhou, Y. Chen and J. Gu, fastp: an ultra-fast all-in-one FASTQ preprocessor, *Bioinformatics*, 2018, **34**(17), i884–i890.

23 D. Kim, B. Langmead and S. L. Salzberg, HISAT: a fast spliced aligner with low memory requirements, *Nat. Methods*, 2015, **12**(4), 357–360.

24 Y. Liao, G. K. Smyth and W. Shi, featureCounts: an efficient general purpose program for assigning sequence reads to genomic features, *Bioinformatics*, 2014, **30**(7), 923–930.

25 M. I. Love, W. Huber and S. Anders, Moderated estimation of fold change and dispersion for RNA-seq data with DESeq2, *Genome Biol.*, 2014, **15**(12), 550.

26 M. Stephens, False discovery rates: a new deal, *Biostatistics*, 2017, **18**(2), 275–294.

27 Y. Afshar, F. Ma, A. Quach, A. Jeong, H. L. Sunshine and V. Freitas, *et al.*, Transcriptional drifts associated with environmental changes in endothelial cells, *eLife*, 2023(12), e81370.

28 G. Yu, L. G. Wang, Y. Han and Q. Y. He, clusterProfiler: an R Package for Comparing Biological Themes Among Gene Clusters. OMICS: A Journal of, *Integr. Biol.*, 2012, **16**(5), 284–287.

29 S. Durinck, P. T. Spellman, E. Birney and W. Huber, Mapping identifiers for the integration of genomic datasets with the R/Bioconductor package biomaRt, *Nat. Protoc.*, 2009, **4**(8), 1184–1191.

30 H. Wickham, M. Averick, J. Bryan, W. Chang, L. McGowan and R. François, *et al.*, Welcome to the Tidyverse, *JOSS*, 2019, **4**(43), 1686.

31 K. Moise, K. M. Arun, M. Pillai, J. Salvador, A. S. Mehta and Y. Goyal, *et al.*, Endothelial cell elongation and alignment in response to shear stress requires acetylation of microtubules, *Front. Physiol.*, 2024(15), 1425620.

32 K. Miyazawa, Y. Itoh, H. Fu and K. Miyazono, Receptor-activated transcription factors and beyond: multiple modes of Smad2/3-dependent transmission of TGF-β signaling, *J. Biol. Chem.*, 2024, **300**(5), 107256.

33 S. Alibrandi, C. Rinaldi, S. L. Vinci, A. Conti, L. Donato and C. Scimone, *et al.*, Mechanotransduction in Development: A Focus on Angiogenesis, *Biology*, 2025, **14**(4), 346.

34 J. Heinke, L. Wehofsits, Q. Zhou, C. Zoeller, K. M. Baar and T. Helbing, *et al.*, BMPER Is an Endothelial Cell Regulator and Controls Bone Morphogenetic Protein-4–Dependent Angiogenesis, *Circ. Res.*, 2008, **103**(8), 804–812.

35 H. Bai, Y. Gao, M. Arzigian, D. M. Wojchowski, W. Wu and Z. Z. Wang, BMP4 regulates vascular progenitor development in human embryonic stem cells through a smad-dependent pathway, *J. Cell. Biochem.*, 2010, **109**(2), 363–374.

36 C. Hiepen, M. Benamar, J. Barrasa-Fano, M. Condor, M. Ilhan and J. Münch, *et al.*, Endothelial tip-cell position, filopodia formation and biomechanics require BMPR2 expression and signaling, *Commun. Biol.*, 2025, **8**(1), 21.

37 P. L. Mendez, L. Raaz, J. Jatzlau, Y. Xiao, P. Vrancaert and J. Ksiazkiewicz, *et al.*, Atheroprone Flow Activates SMAD-FOXO1 to Drive Endothelial-to-Mesenchymal Transition and Atherosclerosis, *bioRxiv*, 2024, preprint, DOI: **10.1101/2024.11.25.625323**.
38 E. Van Haaften, C. Bouten and N. Kurniawan, Vascular Mechanobiology: Towards Control of In Situ Regeneration, *Cells*, 2017, **6**(3), 19.
39 N. Choublier, M. Taghi, M. C. Menet, M. Le Gall, J. Bruce and P. Chafey, *et al.*, Exposure of human cerebral microvascular endothelial cells hCMEC/D3 to laminar shear stress induces vascular protective responses, *Fluids Barriers CNS*, 2022, **19**(1), 41.
40 N. Ohura, K. Yamamoto, S. Ichioka, T. Sokabe, H. Nakatsuka and A. Baba, *et al.*, Global Analysis of Shear Stress-Responsive Genes in Vascular Endothelial Cells, *JAT*, 2003, **10**(5), 304–313.
41 S. J. Kunnen, T. B. Malas, C. M. Semeins, A. D. Bakker and D. J. M. Peters, Comprehensive transcriptome analysis of fluid shear stress altered gene expression in renal epithelial cells, *J. Cell. Physiol.*, 2018, **233**(4), 3615–3628.
42 P. F. Davies, C. F. Dewey, S. R. Bussolari, E. J. Gordon and M. A. Gimbrone, Influence of hemodynamic forces on vascular endothelial function. In vitro studies of shear stress and pinocytosis in bovine aortic cells, *J. Clin. Invest.*, 1984, **73**(4), 1121–1129.
43 T. Kadohama, K. Nishimura, Y. Hoshino, T. Sasajima and B. E. Sumpio, Effects of different types of fluid shear stress on endothelial cell proliferation and survival, *J. Cell. Physiol.*, 2007, **212**(1), 244–251.
44 Y. J. Sei, S. I. Ahn, T. Virtue, T. Kim and Y. Kim, Detection of frequency-dependent endothelial response to oscillatory shear stress using a microfluidic transcellular monitor, *Sci. Rep.*, 2017, **7**, 10019, Available from: **https://www.nature.com/articles/s41598-017-10636-z**.
45 W. A. Muller, Leukocyte-Endothelial Cell Interactions in the Inflammatory Response, *Lab. Invest.*, 2002, **82**(5), 521–533.
46 J. M. Cook-Mills, M. E. Marchese and H. Abdala-Valencia, Vascular Cell Adhesion Molecule-1 Expression and Signaling During Disease: Regulation by Reactive Oxygen Species and Antioxidants, *Antioxid. Redox Signaling*, 2011, **15**(6), 1607–1638.
47 T. Helbing, R. Rothweiler, E. Ketterer, L. Goetz, J. Heinke and S. Grundmann, *et al.*, BMP activity controlled by BMPER regulates the proinflammatory phenotype of endothelium, *Blood*, 2011, **118**(18), 5040–5049.
48 Y. Zhang and H. Wang, Integrin signalling and function in immune cells, *Immunology*, 2012, **135**(4), 268–275.
49 L. Kaltenbach, P. Martzloff, S. K. Bambach, N. Aizarani, M. Mihlan and A. Gavrilov, *et al.*, Slow integrin-dependent migration organizes networks of tissue-resident mast cells, *Nat. Immunol.*, 2023, **24**, 915–924, Available from: **https://www.nature.com/articles/s41590-023-01493-2**.
50 M. Kretschmer, D. Rüdiger and S. Zahler, Mechanical Aspects of Angiogenesis, *Cancers*, 2021, **13**(19), 4987.
51 P. Lu, K. Takai, V. M. Weaver and Z. Werb, Extracellular Matrix Degradation and Remodeling in Development and Disease, *Cold Spring Harbor Perspect. Biol.*, 2011, **3**(12), a005058–a005058.
52 J. Winkler, A. Abisoye-Ogunniyan, K. J. Metcalf and Z. Werb, Concepts of extracellular matrix remodelling in tumour progression and metastasis, *Nat. Commun.*, 2020, **11**(1), 5120.
53 R. Siddhartha and M. Garg, Interplay Between Extracellular Matrix Remodeling and Angiogenesis in Tumor Ecosystem, *Mol. Cancer Ther.*, 2023, **22**(3), 291–305.
54 T. Polk, S. Schmitt, J. L. Aldrich and D. S. Long, Human dermal microvascular endothelial cell morphological response to fluid shear stress, *Microvasc. Res.*, 2022, **143**, 104377.
55 Y. W. Lu, N. Martino, B. D. Gerlach, J. M. Lamar, P. A. Vincent and A. P. Adam, *et al.*, MEF2 (Myocyte Enhancer Factor 2) Is Essential for Endothelial Homeostasis and the Atheroprotective Gene Expression Program, *ATVB*, 2021, **41**(3), 1105–1123.
56 C. L. Karthika, V. Venugopal, B. J. Sreelakshmi, S. Krithika, J. M. Thomas and M. Abraham, *et al.*, Oscillatory shear stress modulates Notch-mediated endothelial mesenchymal plasticity in cerebral arteriovenous malformations, *Cell. Mol. Biol. Lett.*, 2023, **28**(1), 22.
57 C. Park, T. M. Kim and A. B. Malik, Transcriptional Regulation of Endothelial Cell and Vascular Development, *Circ. Res.*, 2013, **112**(10), 1380–1400.
58 B. Chaube, K. M. Citrin, M. Sahraei, A. K. Singh, D. S. De Urturi and W. Ding, *et al.*, Suppression of angiopoietin-like 4 reprograms endothelial cell metabolism and inhibits angiogenesis, *Nat. Commun.*, 2023, **14**(1), 8251.
59 N. Wettschureck, B. Strilic and S. Offermanns, Passing the Vascular Barrier: Endothelial Signaling Processes Controlling Extravasation, *Physiol. Rev.*, 2019, **99**(3), 1467–1525.
60 A. M. Ghaleb and V. W. Yang, Krüppel-like factor 4 (KLF4): What we currently know, *Gene*, 2017, **611**, 27–37.
61 M. Autiero, J. Waltenberger, D. Communi, A. Kranz, L. Moons and D. Lambrechts, *et al.*, Role of PlGF in the intra- and intermolecular cross talk between the VEGF receptors Flt1 and Flk1, *Nat. Med.*, 2003, **9**(7), 936–943.
62 T. Helbing, G. Wiltgen, A. Hornstein, E. Z. Brauers, L. Arnold and A. Bauer, *et al.*, Bone Morphogenetic Protein-Modulator BMPER Regulates Endothelial Barrier Function, *Inflammation*, 2017, **40**(2), 442–453.
63 F. Itoh, Promoting bone morphogenetic protein signaling through negative regulation of inhibitory Smads, *EMBO J.*, 2001, **20**(15), 4132–4142.
64 M. R. Kulikauskas, S. X and V. L. Bautch, The versatility and paradox of BMP signaling in endothelial cell behaviors and blood vessel function, *Cell. Mol. Life Sci.*, 2022, **79**(2), 77.
65 M. Busek, A. Aizenshtadt, T. Koch, A. Frank, L. Delon and M. A. Martinez, *et al.*, Pump-less, recirculating organ-on-a-chip (rOoC) platform, *Lab Chip*, 2023, **23**(4), 591–608.
66 F. Zhang, D. S. Y. Lin, S. Rajasekar, A. Sotra and B. Zhang, Pump-Less Platform Enables Long-Term Recirculating Perfusion of 3D Printed Tubular Tissues, *Adv. Healthcare Mater.*, 2023, **12**(27), 2300423.

